

Cover Page



Universiteit Leiden



The handle <http://hdl.handle.net/1887/138650> holds various files of this Leiden University dissertation.

Author: Junaid, A.O.

Title: Microengineered human blood vessels for next generation drug discovery

Issue date: 2020-12-16

Chapter V

Metabolic response of blood vessels to TNF α

Abidemi Junaid, Johannes Schoeman, Wei Yang, Wendy Stam, Alireza Mashaghi,
Anton Jan van Zonneveld, Thomas Hankemeier

eLIFE (2020) **9**, e54754

Chapter V

Abstract

TNF α signaling in the vascular endothelium elicits multiple inflammatory responses that drive vascular destabilization and leakage. Bioactive lipids are main drivers of these processes. *In vitro* mechanistic studies of bioactive lipids have been largely based on two-dimensional endothelial cell cultures that, due to lack of laminar flow and the growth of the cells on non-compliant stiff substrates, often display a pro-inflammatory phenotype. This complicates the assessment of inflammatory processes. Three-dimensional microvessels-on-a-chip models provide a unique opportunity to generate endothelial microvessels in a more physiological environment. Using an optimized targeted liquid chromatography–tandem mass spectrometry measurements of a panel of pro- and anti-inflammatory bioactive lipids, we measure the profile changes upon administration of TNF α . We demonstrate that bioactive lipid profiles can be readily detected from three-dimensional microvessels-on-a-chip and display a more dynamic, less inflammatory response to TNF α , that resembles more the human situation, compared to classical two-dimensional endothelial cell cultures.

V

Introduction

Tumor necrosis factor- α (TNF α) is a central mediator of the inflammatory response[1]. TNF α can be generated by monocytes or macrophages and activates endothelial cells at sites of tissue injury or infection through TNF receptor-1 (TNFR1)[2-4]. Following activation, the endothelium elicits a multitude of local responses such as vascular leakage, leukocyte adhesion and coagulation that together are essential to the physiological homeostatic responses to anti-microbial immunity.

However, chronic exposure to adverse metabolic and hemostatic risk factors[5], obesity[6], or disease states such as kidney disease[7] or rheumatoid arthritis[8] are all associated with a systemic inflammatory condition and elevated circulating levels of TNF α . As a consequence, TNF α signaling induces the generation of high levels of free radicals in the vascular endothelium that, when excessive, can deplete the cellular anti-oxidant defense systems and lead to a state of oxidative stress and vascular dysfunction [9].

Mechanistically, TNF α signaling in endothelial cells involves the activation of NF κ B and results in the increased synthesis of reactive oxygen species (ROS) from a number of sources such as mitochondria, NADPH oxidase, uncoupled eNOS, xanthine oxidase, and peroxidases[10, 11]. On its turn, elevated ROS can lead to the generation of bioactive lipids directly or indirectly, such as prostaglandins, isoprostanes, lysophosphatidic acid classes, sphingolipids and platelet activating factor (PAF). Under physiologic conditions, in concert with the transcriptional regulation of a plethora of inflammatory genes[12], these bioactive lipids are critically involved in the first response of endothelial cells to environmental changes, controlling vascular permeability and platelet- and leukocyte adhesion. Also, in fore mentioned patients, isoprostanoids such as 8-epiPGF 2α are generated by peroxidation during conditions of oxidative stress[13] and serve as gold standard oxidative stress plasma markers[14] associating with an increased risk for cardiovascular disease and its underlying causes[15, 16].

The central role of TNF α in many disease states has identified this cytokine as an important therapeutic target to counteract vascular inflammation[1, 17] and several TNF α blockers have been approved by the FDA and have been effective for the suppression of immune-system diseases, such as Crohn's disease, ulcerative colitis, rheumatoid arthritis, ankylosing spondylitis, psoriatic arthritis and plaque psoriasis[18].

Following the success of the TNF α antagonists, a deeper understanding of the impact of oxidative stress on the homeostasis of the human vascular endothelium may yield more specific targets for inflammatory diseases affecting the vasculature. To that end, many *in vitro* mechanistic studies have relied on static, two-dimensional (2D) cultures of primary endothelial cells such as those derived from human umbilical veins (HUVECs)[19]. However, in recent years it has become increasingly apparent that these cultures reflect a ‘stressed’ endothelial phenotype due to the lack of their native environmental cues. *In vitro*, endothelial cells are usually cultured on surfaces such as plastics and glass that are much stiffer than natural substrates such as the extracellular matrix. Recent studies demonstrated that primary endothelial cells on a hard substrate adopt a pro-inflammatory phenotype[20, 21]. Vascular stiffness is strongly associated with vascular disorders such as arterial hypertension, kidney disease and atherosclerosis[22]. Likewise, native microvessels need laminar shear to maintain a quiescent phenotype and the lack of laminar shear stress in static cultures converts endothelial cells to a pro-inflammatory “diseased” phenotype[23].

V

Novel microfluidics-based perfused three-dimensional (3D) microvessels-on-a-chip models provide a unique opportunity to generate endothelial microvessels in a more physiological environment. We employed a gelatin coated 3D microvessels-on-a-chip model in which endothelial cells are organized in a tube-like architecture, with densities of cells and area to volume ratios that are closer to a physiological condition than those in typical 2D culture.

To assess whether these 3D microvessels display a more anti-inflammatory phenotype, we used an optimized targeted liquid chromatography–tandem mass spectrometry measurements of a panel of pro- and anti-inflammatory bioactive lipids and generated expression profiles both in TNF α treated microvessels under flow as well as in 2D endothelial cell cultures under static condition. We demonstrate bioactive lipid profiles can be readily detected from single microvessels and display a more dynamic, less inflammatory response to TNF α , that resembles more the human situation, compared to classical 2D endothelial cell cultures.

Chapter V

Methods

Key resources table

Reagent type (species) or resource	Designation	Source or reference	Identifiers	Additional information
biological sample (include species here)	primary human umbilical vein endothelial cells	Leiden University Medical Center (LUMC)		freshly isolated from umbilical cord of male newborns
chemical compound, drug	phorbol 12-myristate 13-acetate	Sigma-Aldrich	Cat#:P8139	
peptide, recombinant protein	tumor necrosis factor- α	Sigma-Aldrich	Cat#:H8916	
biological sample (include species here)	rat tail collagen type 1	Trevigen	Cat#:3440-005-01	
antibody	mouse anti-human CD144	BD Biosciences	Cat#:555661; RRID:AB_396015	IF(1:150)
antibody	sheep anti-human CD31	R&D Systems	Cat#:AF806; RRID:AB_355617	IF(1:150)
antibody	rabbit anti-human vWF	Agilent Dako	Cat#:A0082; RRID:AB_2315602	IF(1:1000)
antibody	alexa fluor 488-conjugated goat anti-mouse	ThermoFisher	Cat#:R37120; RRID:AB_2556548	IF(1:250)
antibody	alexa fluor 488-conjugated donkey anti-sheep	ThermoFisher	Cat#:A11015; RRID:AB_141362	IF(1:250)



Reagent type (species) or resource	Designation	Source or reference	Identifiers	Additional information
antibody	alexa fluor 647-conjugated goat anti-rabbit	ThermoFisher	Cat#:A27040; RRID:AB_2536101	IF(1:250)
other	rhodamine phalloidin	Sigma-Aldrich	Cat#:P1951; RRID:AB_2315148	IF(1:200)
other	hoechst	Invitrogen	Cat#:H3569; RRID:AB_2651133	IF(1:2000)
software, algorithm	LabSolutions	Shimadzu	RRID:SCR_018241	
software, algorithm	SPSS	SPSS	RRID:SCR_002865	
software, algorithm	GraphPad Prism	GraphPad	RRID:SCR_002798	

Cell culture

Human umbilical vein endothelial cells (HUVECs) were isolated from umbilical cord of newborns, collected with informed consent, by an adaption of the method developed by Jaffe et al. in 1973 [19]. Although denoted as veins, umbilical veins carry oxygenated blood and thus the phenotype of their endothelium is similar to arterial endothelial cells.

The umbilical cord was severed from the placenta soon after birth and placed in a sterile container filled with phosphate-buffered saline (PBS; Fresenius Kabi, The Netherlands) and held at 4°C until processing. The cord was inspected and at both ends a piece of 1 cm was cut off to remove damaged tissue from clamping. Subsequently, the umbilical vein was cannulated and perfused with PBS to wash out the blood and allowed to drain. When clear fluid flow was observed, the vein was filled with trypsin/EDTA solution (CC-5012, Lonza, USA), placed in the container filled with PBS and incubated at 37°C for 20 min. After incubation, the trypsin-EDTA solution containing the endothelial cells was flushed from the cord with air and afterwards PBS. The effluent was collected in a sterile 50 ml tube containing 20 ml Endothelial Cell Growth Medium 2 (EGM2; C-39216, PromoCell, Germany) supplemented with antibiotics and the cell suspension was centrifuged at 1200 rpm for 7 min. The cell pellet was

Chapter V

resuspended in 10 ml EGM2 and cultured on 1% gelatin-coated T75 flasks. Cells were maintained in a 37°C incubator with 5% CO₂ and the medium was refreshed every other day. After 80% confluency, cells were split at 1:3 ratio and cultured in new 1% gelatin-coated T75 flasks. The isolated cells were positive for the endothelial cell markers, including platelet endothelial cell adhesion molecule (PECAM-1) and von Willebrand factor (vWF) (Figure 1). All experiments using HUVECs were repeated 6 times using cells from 3 different male donors at passage 3.

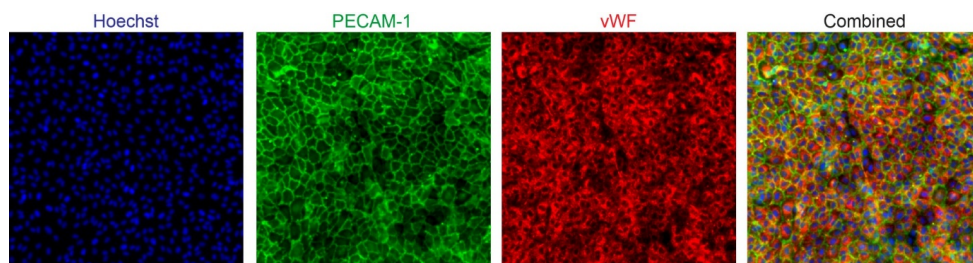


Figure 1 | Expression of platelet endothelial cell adhesion molecule (PECAM-1) and von Willebrand factor (vWF) in isolated human umbilical vein endothelial cells (HUVECs).

For 2D experiments, we cultured $50 \cdot 10^3$ cells/ml in 24-well plates overnight at 37 °C in humidified air containing 5% CO₂. The following day, the cells were incubated with 15 and 50 ng/ml TNF α (H8916, Sigma-Aldrich, The Netherlands) and 20 ng/ml phorbol 12-myristate 13-acetate (PMA; P8139, Sigma-Aldrich, The Netherlands) for 18 hours. The medium was collected and stored in -80°C.

We used the OrganoPlate (9603-400-B, MIMETAS, The Netherlands) for all microfluidic cell culture experiments. The microvascular and extracellular matrix (ECM) channels were separated by phaseguides [53]. Before seeding the cells, 4 mg/ml rat tail collagen type 1 (3440-005-01, Trevigen, USA) neutralized with 10% 37 g/L Na₂CO₃ (S5761, Sigma-Aldrich, The Netherlands) and 10% 1 M HEPES buffer (15630-056, Gibco, The Netherlands) was added in the ECM channels. Subsequently, the collagen was let to polymerize by incubating the device for 10 min in the incubator at 37°C and 5% CO₂. The observation windows were filled with 50 μ l Hank's Balanced Salt Solution with calcium and magnesium buffers (HBSS+; 24020117, Life

Technologies, The Netherlands) for optical clarity and to prevent gel dehydration. Using a repeater pipette, 2 μl of 1% gelatin was added into the inlet of each microvascular channel and the device was put in the incubator at 37°C for 30 min. We trypsinized cells at 80-90% confluency and seeded $15 \cdot 10^6$ cells/ml in the outlet of the microvascular channels of the OrganoPlate. Afterwards, the cells were incubated at 37°C and 5% CO₂ for one hour to allow microvascular formation. After incubation, 50 μl of culture medium was added to the inlets and outlets of the microvascular channels. The device was placed on a rocker platform with a 7° angle of motion and an eight-minute timed operation to allow continuous flow of minor volumes of medium in the microvessels. The microvascular channels typically contain volumes of < 1 μl . After 24 hours, the medium was refreshed, and the HUVECs were cultured for an additional 3-4 days. The microvessels were treated with TNF α (0.4, 15 and 50 ng/ml) and PMA (20 ng/ml) for 18 hours. Subsequently, medium of four microvessels were pooled to form one sample to allow analyses of metabolites at low concentrations due to low cell numbers. This still allowed us to create three biological replicates with 4 – 6 technical replicates data per experimental condition for metabolomics analyses. The samples were stored in -80°C.

V

Immunofluorescence staining

For immunofluorescence staining, HUVECs were fixed using 4% paraformaldehyde (PFA) in HBSS+ for 10 min at room temperature. The fixative was aspirated, and the cells were rinsed once with HBSS+. Next, the cells were permeabilized for 2 min with 0.2% Triton X-100 in HBSS+ and washed once with HBSS+. The cells were blocked in 5% BSA in HBSS+ for 30 min and incubated with the primary antibody solution overnight at 4°C. Mouse anti-human CD144 (1:150; 555661, BD Biosciences, USA), sheep anti-human CD31 (1:150; AF806, R&D Systems, The Netherlands) and rabbit anti-human vWF (1:1000; A0082, Agilent Dako, USA) were used as the primary antibodies. The cells were washed with HBSS+, followed by an one-hour incubation with Hoechst (1:2000; H3569, Invitrogen, USA), rhodamine phalloidin (1:200; P1951, Sigma-Aldrich, The Netherlands) and the secondary antibody solution, containing Alexa Fluor 488-conjugated goat anti-mouse (1:250; R37120, ThermoFisher, USA), Alexa Fluor 488-conjugated donkey anti-sheep (1:250; A11015, ThermoFisher, USA) and Alexa Fluor 647-conjugated goat anti-rabbit (1:250; A27040, ThermoFisher, USA) antibodies. The cells were

washed three times with HBSS+. High-quality Z-stack images of the stained cells were acquired using a high-content confocal microscope (Molecular Devices, ImageXpress Micro Confocal).

Metabolic profiling

All samples were measured using an oxidative and nitrosative stress profiling platform which has been developed and validated in our lab [28]. This platform covers various isoprostane classes, signaling lipids from the sphingosine and sphinganine classes and their phosphorylated forms, as well as three classes of lysophosphatidic acids: lysophosphatidic acids, alkyl-lysophosphatidic acids and cyclic-lysophosphatidic acids (all ranging from C14 to C22 chain length species). For metabolite extraction, sample preparation procedure was according to the in-house experimental protocol which has been standardized and published; extra samples were pooled for internal quality control (QC) [28]. Briefly, cell media (150 μ l) were thawed on ice and added with 5 μ l antioxidant solution and 10 μ l internal standards (ISTDs). Acidified with citric acid/phosphate buffer (pH 4.5), all samples were then dealt with liquid-liquid extraction (LLE) with 1 mL of butanol and ethyl acetate (1:1 v/v). Samples were vortexed and centrifuged and then the organic phase was collected and dried. After reconstitution with ice-cold 70% MeOH injection solution, each sample was again vortexed and centrifuged and the supernatant was transferred to the insert in a glass vial. Ultra-performance liquid chromatography tandem mass spectrometry (UPLC-MS/MS) based analysis was then applied for low-pH measurement (Shimadzu LCMS-8060, Japan) and high-pH measurement (Shimadzu LCMS-8050, Japan) respectively.

Calibration curve preparation

Standard stock solutions were prepared in MeOH containing butylated hydroxytoluene (0.4 mg/ml). A calibration stock was made with concentrations found in Supplementary Table 1 for the prostaglandins, isoprostanes, LPAs, sphingolipids and PAF available base standards and was labeled "C9". This solution was diluted to levels C8 to C1 and from these mixes, 20 μ l was added to 150 μ l sample to construct the calibration curves.

Data pre-processing

LabSolutions (Shimadzu, Version 5.91) was applied to accomplish all the peak determination and integration. For each metabolite, the response ratio was obtained by calculating the ratio of peak area of the target compound to the peak area of the assigned internal standard. After QC evaluation, metabolites of which QC samples had an RSD less than 30% were used for further statistical analysis. Finally, the absolute concentration of the targets was determined using the calibration curves.

Statistical analysis

Heatmaps and bar plots were created with GraphPad Prism 7 (GraphPad Software). The fold change was calculated by normalizing the conditions to the control group. Subsequently, the data was log₂ transformed and used for the heatmaps. The absolute concentration of those compounds were visualized in the bar plots. We used IBM SPSS Statistics 23 (IBM) for statistical analyses. Bar plots were plotted as mean ± s.e.m. of three biological replicates per condition; n = 4 – 6 technical replicates. Significance levels were set at *P<0.1, **P<0.05, ***P < 0.01, ****P < 0.001 using the unpaired Student's t-test.

Results and discussion

Bioactive lipids generated by 3D microvessels-on-a-chip can be measured by UPLC-MS/MS

In this paper, we present a novel set-up to measure the metabolic response of 3D endothelial microvessels to TNF α , including pro- and anti-inflammatory markers. We cultured 96 perfused microvessels against extracellular matrix (ECM) using the microvessels-on-a-chip platform technology recently developed by using the OrganoPlate platform of MIMETAS[24, 25]. The microchannels in the OrganoPlate were coated with gelatin, preventing endothelial cells from growing on glass and enabling them to form stable microvessels. The shear stress in the microvessels, calculated based on a previous work, ranges from 1-5 dyne/cm² [26]. *In vivo*, the shear stress ranges from 95.5 dyne/cm² at the smallest capillaries to 2.8 dyne/cm² at the

postcapillary venules[27]. Conditioned medium perfused through TNF α treated and control (untreated) microvessels was sampled, pooled and measured with a UPLC-MS/MS metabolomics method developed recently by us to study inflammation and oxidative stress (Figure 2)[28].

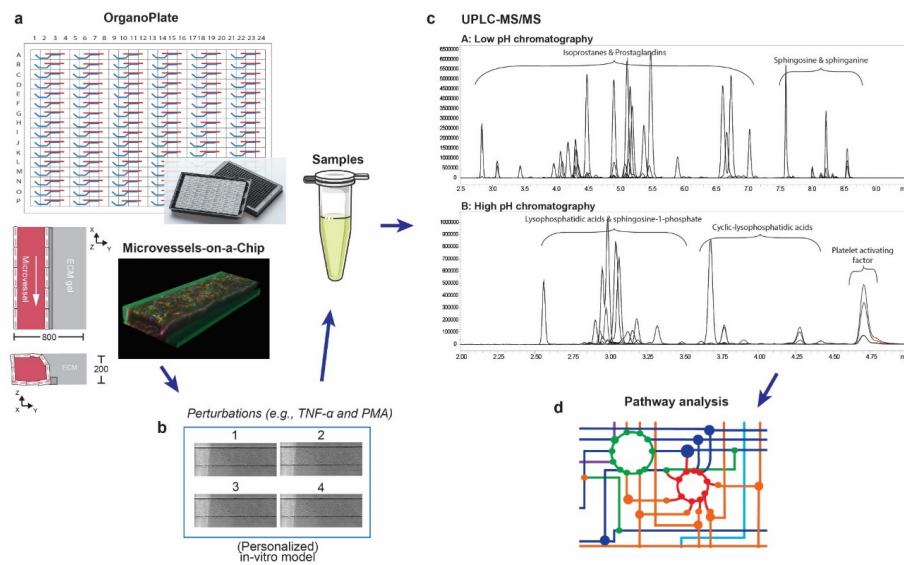


Figure 2 | Metabolomics workflow. (a) Schematic diagram of the OrganoPlate 2-lane design and 3D reconstruction of the microvessels-on-a-chip formed by cultured HUVECs (blue: Hoechst, red: F-actin and green: VE-cadherin). All dimensions are in μm . (b) Collection of culture media after perfusion. The medium of four microvessels were pooled to form one sample. (c) Identification and quantification of prostaglandins, isoprostanes, lysophosphatidic acid (LPA) classes, sphingolipids and platelet activating factor (PAF) in microvessels-on-a-chip by UPLC-MS/MS using two different solvent gradients. (d) Pathway analysis.

As a metabolic read-out for TNF α signaling, we measured prostaglandins, isoprostanes, LPAs, lysosphingolipids and PAF and first assessed the concentrations of these metabolites in the basic EGM2 medium and compared their concentrations after 18 hours incubation to condition the medium in the microvessels-on-a-chip cultures. As shown in Table 1, the peaks detected demonstrated that, while members of the prostaglandins and isoprostanes clearly increased after conditioning of the medium, most of the LPA metabolites were readily

Chapter V

detectable in the medium and actually displayed a significant decreased concentration. When the EGM2 medium was incubated for 18 hours without exposure to the microvessels no significant changes in the concentrations of these metabolites was observed. Therefore, we conclude that during the conditioning of the medium, prostaglandins and isoprostanoids are excreted from the endothelial cells and that the LPA metabolites are consumed or actively degraded by the cells.

Table 1 | The peak area ratio of metabolites in the culture medium (EGM2) normalized with the peak area ratio of metabolites found in the culture medium after perfusion in the microvessels-on-a-chip for 18 hours (EGM2 HUVECs). The peak area ratio is the peak area of the metabolites divided by the appropriate peak area of the internal standards. Fold changes below the 1 (blue) and above the 1 (red) indicates that low and high concentrations of fatty acids were present in medium before exposure to the microvessels. The data represents one biological replicate; n = 3 technical replicates.

Bioactive lipid*	EGM2/EGM2 HUVECs	Bioactive lipid*	EGM2/EGM2 HUVECs
PGF2 α	0.1	LPA C22:5	18.2
PGF3 α	2.1	LPA C16:0	21.3
8-iso-13, 14-dihydro-PGF2 α	0.0	LPA C18:1	48.4
8-iso-PGF2 α	0.2	LPA C22:4	5.9
5-iPF2 α	0.4	cLPA C20:4	78.6
8, 12-iPF2 α IV	0.5	LPA C18:0	0.0
LPA C14:0	6.2	cLPA C18:2	0.0
LPA C16:1	25.4	cLPA C16:0	14.8
LPA C22:6	17.7	cLPA C18:1	25.8
LPA C18:2	77.2	cLPA C18:0	11.1
LPA C20:4	31.0	S-1-P C18:1	0.9

*The rest of the metabolites shown in Figure 4 are not displayed, because they were not detected in the EGM2.

When we assessed the biolipid composition of the conditioned medium of TNF α stimulated microvessels, 33 measured metabolites passed the quality control (QC) thresholds. Figure 3 shows examples of the chromatograms of prostaglandin E2 and different isoprostanoid isomers that were secreted by the microvessels after exposure to TNF α for 18 hours compared to the control samples showing a marked increase in abundance of a number of these metabolites. The control samples are microvessels without exposure to TNF α .

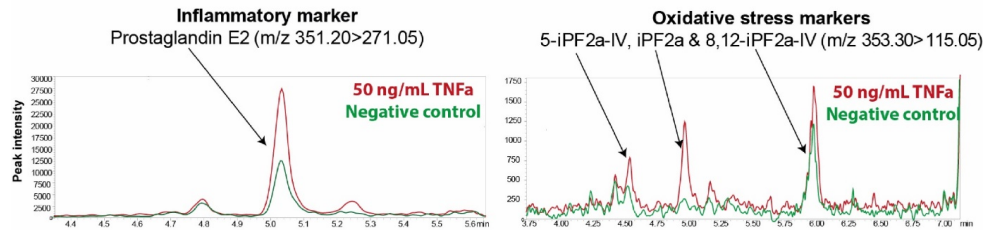


Figure 3 | Inflammatory and oxidative stress markers in microvessels-on-a-chip. Reconstructed LC-MS/MS ion chromatograms of PGE2, 5-iPF2 α IV, iPF2 α and 8, 12-iPF2 α IV in microvessels treated with 50 ng/ml TNF α for 18 hours.

Bar plots of the absolute concentrations of prostaglandins are presented in Figure 4a, showing a significant difference between untreated and TNF α treated microvessels. While at physiological concentration of TNF α (0.4 ng/ml) there was an increase in the excretion of PGF1 α , PGF2 α , PGF3 α , PGE2, PGD2 and 13, 14-dihydro-PGF2 α , however, no significant difference between the untreated and TNF α treated microvessels was evident, except for PGF1 α . At 15 ng/ml a stronger differential response was observed for selected isoprostanes, several LPAs, sphingolipids and PAF (Figure 4b-e). The relative concentrations of the bioactive lipids found in the microvessels-on-a-chip are strikingly similar with those found in normal human blood vessels (Table 2).



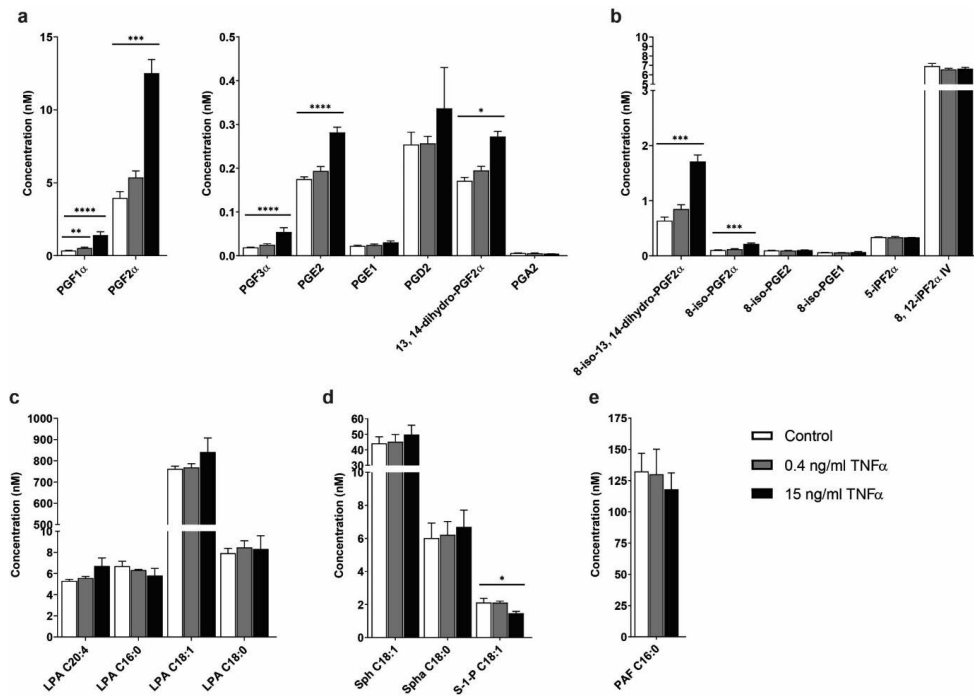


Figure 4 | TNF α -induced concentration profile changes of the signaling lipids in the microvessels-on-a-chip. Concentrations of (a) prostaglandins, (b) isoprostanes, (c) lysophosphatidic acid (LPA) classes, (d) sphingolipids and (e) platelet activating factor (PAF) with available standards detected in the microvessels without TNF α exposure (control) and after exposure to 0.4 and 15 ng/ml TNF α for 18 hours. Data represent mean and s.e.m. of three biological replicates per condition; n = 4 – 6 technical replicates. Significance determined by unpaired Student's t-test; *P<0.1, **P<0.05, ***P < 0.01, ****P < 0.001

Chapter V

Table 2 | Comparison of the concentration of bioactive lipids between living human blood vessel and human microvessels-on-a-chip. The concentrations in human blood vessel were obtained from HMDB[54-57].

Bioactive lipid	Human blood vessel		Microvessels-on-a-chip	
	Healthy	Diseased	Healthy	Diseased
PGF1 α	-0.0317 - 0.376 nM	-	~0.350 nM	-0.527 - 1.412 nM
PGF2 α	-0.144 - 0.371 nM	~ 0.4 - 1.6 nM	~3.96 nM	~5.36 - 12.5 nM
PGE2*	~0.13 - 0.172 nM	-	~0.175 nM	-0.194 - 0.281 nM
PGE1	< 0.1 nM	-	~0.0225 nM	~0.0246 - 0.0308 nM
PGD2	~0.065 - 0.2 nM	-	~0.254 nM	~0.257 - 0.336 nM
PGA2	~0.0448 - 0.496 nM	-	~0.006 nM	~0.0048 - 0.0058 nM
8-iso-PGF2 α	~0.057 - 0.57 nM	-	~0.103 nM	~0.122 - 0.216 nM
S-1-P C18:1	~0.5 - 3.0 nM	-	~2.12 nM	~1.47 - 2.11 nM
Sph C18:1	~1.3 - 50 nM	-	~44.2 nM	~45.2 - 49.8 nM
Spha C18:0	~1.3 - 50 nM	-	~6.0 nM	~6.2 - 6.7 nM

Phorbol 12-myristate 13-acetate (PMA) is an activator of protein kinase C (PKC), hence of NF κ B, that relates to TNF α signaling and causes a wide range of effects in cells. As it is a known and potent up-regulator of cyclooxygenase-2 (COX-2) [29], we next measured the effect of PMA on the secretion of the biolipids to compare the TNF α response to a condition of maximal stimulation. When our combined results were plotted in a heatmap, marked differences are observed between control- and TNF α or PMA-treated microvessels (Table 3).



Chapter V

Table 3 | Heatmap of prostaglandins, isoprostanes, lysophosphatidic acid (LPA) classes, sphingolipids and platelet activating factor (PAF) detected in the microvessels-on-a-chip.

	Bioactive lipid	Fold change of concentration			Inflammatory action	Platelet activation	Vascular tone	Angiogenic action
		15 ng/ml TNF	50 ng/ml TNF	20 ng/ml PMA				
Prostaglandins	PGF1 α	2.0	1.8	5.0	anti	no	con	
	PGF2 α	1.7	1.5	5.0	pro	no	con	pro
	PGF3 α	1.5	1.1	4.4	anti			
	PGE2*	0.7	0.7	3.7	pro	anti	dil	pro
	PGE1	0.5	0.4	2.7	anti	anti	dil	pro
	PGD2	0.4	3.4	3.5	anti	anti	con	anti
	13, 14-dihydro-PGF2 α	0.7	0.5	2.3	pro			
	PGA2	-0.3	0.0	2.6	anti	no		
Isoprostanes	8-iso-13, 14-dihydro-PGF2 α	1.4	1.3	4.6				anti
	8-iso-PGF2 α *	1.1	0.9	4.2	pro	anti	con	anti
	8-iso-PGE2	0.1	0.0	2.1	pro	anti	con	anti
	8-iso-PGE1	0.1	0.0	0.7		anti	con	anti
	5-iPF2 α	0.0	0.0	0.0				
	8, 12-iPF2 α IV	-0.1	0.0	0.2				
Lysophosphatidic acids	LPA C14:0	-0.2	-0.2	-0.4	pro	pro	con	pro
	LPA C16:1	-0.4	-0.3	-0.6	pro	pro	con	pro
	LPA C22:6*	0.4	0.5	0.2	pro	pro	con	pro
	LPA C18:2	0.1	0.0	-0.1	pro	pro	con	pro
	LPA C20:4	0.3	0.4	0.3	pro	pro	con	pro
	LPA C22:5*	0.5	0.6	0.3	pro	pro	con	pro
	LPA C16:0	-0.2	-0.3	-0.3	pro	pro	con	pro
	LPA C18:1	0.1	0.2	-0.1	pro	pro	con	pro
	cLPA C20:4	-0.1	-0.2	-0.1	anti	anti	no	
	LPA C18:0	0.1	0.0	-0.2	pro	pro	con	pro
	cLPA C16:0	-0.2	0.0	0.0	anti	anti	no	
	cLPA C18:0	-0.2	-0.1	-0.2	anti	anti	no	
Sphingolipids	S-1-P C18:1	-0.5	-0.6	-0.9	anti	anti	con	pro
	Sph C18:1	0.2	0.1	0.0	anti	anti	con	pro
	Spha C18:0	0.2	0.0	-0.1				
	PAF C16:0	-0.2	-0.2	-0.4	pro	pro	con	pro

The fold changes were measured with respect to the controls and log2 transformed. The controls are microvessels unexposed to TNF α and PMA. The metabolites are characterized by their inflammatory action (anti- or pro-inflammatory), platelet activation (anti- or pro-platelet activation), vascular tone (constriction or dilation) and angiogenic action (anti- or pro-angiogenic). The data was obtained from the experiments done in Figure 4

with three biological replicates per condition; n = 4 – 6 technical replicates. *Validated markers of oxidative stress.

Impact of TNF α on prostaglandin levels

As shown in Table 3, overnight exposure to TNF α and PMA shows increase in the release of the prostaglandins PGF1 α , PGF2 α , PGF3 α , PGE2, PGD2 and 13, 14-dihydro-PGF2 α from the TNF α treated microvessels (Figure 4a and Table 3). During inflammation, ROS contributes to the increased PGE2, PGF2 α , PGD2 and 13, 14-dihydro-PGF2 α production through the release of arachidonic acid and COX-2 activation, having a pro-inflammatory effect in the endothelium[30, 31]. At the same time, anti-inflammatory prostaglandins PGF1 α , PGF3 α , PGE1, and PGA2 are also secreted by the endothelium[32, 33]. PGE1 and PGA2 are known to suppress TNF α induced NF κ B activation and production of ROS[34]. Relating to these two prostaglandins, no differences were detected in our system between untreated and TNF α treated microvessels for 18 hours.

Impact of TNF α on isoprostane levels

When we focus on the compounds produced by the reaction of free radicals with arachidonic acid, the isoprostanes, high levels of 8-iso-13, 14-dihydro-PGF2 α and 8-iso-PGF2 α were detected in the supernatant of TNF α treated microvessels (Figure 4b and Table 3). These metabolites inhibit platelet aggregation and induce monocyte adhesion to endothelial cells [35, 36]. We also detected 8-iso-PGE2, 5-iPF2 α , 8, 12-iPF2 α IV and 8-iso-PGE1 in the control sample and TNF α induced microvessels. 8-iso-PGE1 is recognized as vasoconstrictor with a similar effect as PGF2 α [37]. However, no significant difference between the two groups was evident after incubating the microvessels for 18 hours with TNF α .

Impact of TNF α on lysophosphatidic acids, sphingolipids and platelet activating factor

Looking at lipids that mediate diverse biological actions, the LPA classes, sphingosine and PAF are appropriate markers to take along in our metabolic read-out, because of their diverse

biological actions. The LPA classes consist of LPAs and cyclic-lysophosphatidic acids (cLPAs). They are formed by activated platelets and oxidation of low-density lipoproteins (LDLs) [38]. Once an inflammatory response is triggered, LPAs can activate platelets [39] and lead to endothelial dysfunction by activating NF κ B [40-43]. On the other hand, cLPAs inhibit pro-inflammatory cytokine expression in the endothelium [44]. In our data, we saw high concentrations of several LPAs in the control sample compared to TNF α treated microvessels. Similar results were seen in the levels of sphingosine-1-phosphate (S-1-P) and PAF (Table 3 and Figure 4c-e). In TNF α signaling, S-1-P binds to TNF receptor-associated factor 2 (TRAF2) to activate NF κ B, while PAF induces vascular permeability [45, 46].

TNF α induced bioactive lipid profiles from endothelial cells in 3D configuration are less inflammatory compared to 2D monolayers

To assess whether these three-dimensional microvessels display a more anti-inflammatory phenotype, we compared the bioactive lipid response of the 3D microvessels-on-a-chip to TNF α to that of 2D endothelial cell monolayers. In addition, we made a detailed inventory of the reported action of the individual lipids on inflammation, platelet activation, vascular tone and angiogenesis (for references see Supplementary Table 2). When the TNF α -induced biolipids profiles are listed in relation to their biological activities (Table 4) we conclude that the 3D microvessels-on-a-chip display a more dynamic, less inflammatory response to TNF α , that resembles more the human situation, compared to classical 2D endothelial cell cultures. In particular, the anti-inflammatory prostaglandins PGF1 α , PGF3 α , and PGD2 are increased to a larger extent and the anti-inflammatory lysophosphatidic acids are maintained or decreased to a lesser extent. In concert, the pro-inflammatory lipids PGE2, 8-iso-PGE2 and 8-iso-PGF2 α are present at higher levels in the medium of the TNF α exposed 2D endothelial monolayer culture. The elevated levels of the oxidative stress markers PGE2, 8-iso-PGF2 α [14], LPA C22:5 and LPA C22:6[18] confirm the increased inflammatory status of the 2D cultures making it tempting to speculate that an increased production of ROS in these cells may underlie these responses. The response of the microvasculature to inflammatory cytokines such as TNF α is often directly associated with inhibition of platelet activation (to maintain patency of the microvessel), a vasoconstrictive response and a pro-angiogenic response characterized by the

Chapter V

loss of endothelial cell-cell contacts and microvascular leakage. Many of these activities are also driven by the bioactive lipids in our panel (Supplementary Table 2) and it is interesting to note that concomitantly to the less inflammatory nature of the profiles of the conditioned media derived from the 3D microvessel the profile also suggests to be more restrictive of platelet activation, less vasoconstrictive and less angiogenic. It should be noted that we did not compare the excretion of bioactive of unstimulated 2D cell cultures and 3D vessels as the normalization on the number of endothelial cells would not have been straightforward.

V

Chapter V

Table 4 | Heatmap of pro- and anti- inflammatory and oxidative stress markers measured in 3D microvessels-on-a-chip and 2D endothelial cell monolayers.

Bioactive lipid	Fold change of concentration		Inflammatory action	Platelet activation	Vascular tone	Angiogenic action
	2D TNF	3D TNF				
PGF1 α	1.9	3.4	anti	no	con	
PGF3 α	1.0	6.6	anti			
PGE1	2.1	1.9	anti	anti	dil	pro
PGD2	2.3	6.5	anti	anti	con	anti
PGA2	0.7	0.0	anti	no		
cLPA C20:4	-0.7	-0.5	anti	anti	no	
cLPA C18:2	-0.5	0.0	anti	anti	no	
cLPA C16:0	-0.6	-0.3	anti	anti	no	
cLPA C18:1	-0.9	-0.2	anti	anti	no	
cLPA C18:0	-0.6	-0.2	anti	anti	no	
S-1-P C18:1	-2.0	-0.9	anti	anti	con	pro
8-iso-PGE1	1.8	1.9		anti	con	anti
5-iPF2 α	0.3	-0.1				
PGF2 α	1.9	2.2	pro	no	con	pro
PGE2*	2.4	1.0	pro	anti	dil	pro
13, 14-dihydro-PGF2 α	0.9	1.1	pro			
8-iso-13, 14-dihydro-PGF2 α	1.9	1.9				anti
8-iso-PGF2 α *	2.0	1.3	pro	anti	con	anti
8-iso-PGE2	0.6	-0.3	pro	anti	con	anti
LPA C14:0	0.0	-0.8	pro	pro	con	pro
LPA C16:1	-1.0	-1.0	pro	pro	con	pro
LPA C22:6*	0.0	-0.3	pro	pro	con	pro
LPA C18:2	-1.0	-1.2	pro	pro	con	pro
LPA C20:4	-0.2	-0.4	pro	pro	con	pro
LPA C22:5*	1.0	-0.1	pro	pro	con	pro
LPA C16:0	-0.6	-0.6	pro	pro	con	pro
LPA C18:1	-0.5	-1.0	pro	pro	con	pro
LPA C18:0	0.1	-0.9	pro	pro	con	pro
PAF C16:0	-0.5	-0.8	pro	pro	con	pro

The cells were treated with 15 ng/ml TNF α in the same experiment as Figure 4. The fold changes were measured with respect to the controls and log₂ transformed. The controls are microvessels unexposed to TNF α and PMA. The metabolites are characterized by their inflammatory action (anti- or pro-inflammatory), platelet activation (anti- or pro-platelet activation), vascular tone (constriction or dilation) and angiogenic action (anti- or pro-

Chapter V

angiogenic). The data represents one biological replicate; n = 2 – 3 technical replicates. *Validated markers of oxidative stress.

The observed differences between the 2D and the 3D chip-based platforms may be attributed to the mechanical properties of the two systems[47]. The microvessels-on-a-chip are surrounded by an ECM layer and the 3D configuration allows intensified cell-cell interactions, resembling the *in vivo* situation. Moreover, vascular endothelial cells *in vivo* are influenced by distinct hemodynamic forces and this applies also to the endothelial cells in our microvessels-on-a-chip. Evidence suggest that shear stress activates phospholipids turnover that is involved in the production of free arachidonic acid [48]. This might also explain the differences we see between the increase/decrease of fatty acids in the microvessels-on-a-chip and the 2D cell culture. As shear stress influences RhoA activity and stress fiber formation, the regulation of fatty acids, RhoA might be important in this process [49]. In addition, the environmental changes in the 3D configuration could impact on the expression of the TNF receptors.

Several reports showed that oxidative stress induces endothelial dysfunction, which plays a central role in vascular diseases. It can promote the expression of pro-inflammatory and pro-coagulant factors, apoptosis and impair the release of nitric oxide [50, 51]. This study set out with the aim of using metabolomics as a readout of endothelial function in microvessels-on-a-chip exposed to TNF α to trigger inflammatory responses seen in vasculopathy. For the first time we show that the regulation of prostaglandins, isoprostanes, LPAs, sphingolipids and PAF can be measured in our microfluidic system, even though they cause profound physiological effects at very dilute concentrations that serve as early-stage markers of oxidative stress and inflammation [52]. The findings support the model that TNF α signaling induces ROS production that causes changes in signal transduction and gene expression, which leads to release of oxidative stress and inflammatory markers (Figure 5). Further research should be undertaken to confirm the results in gene and protein levels.

V

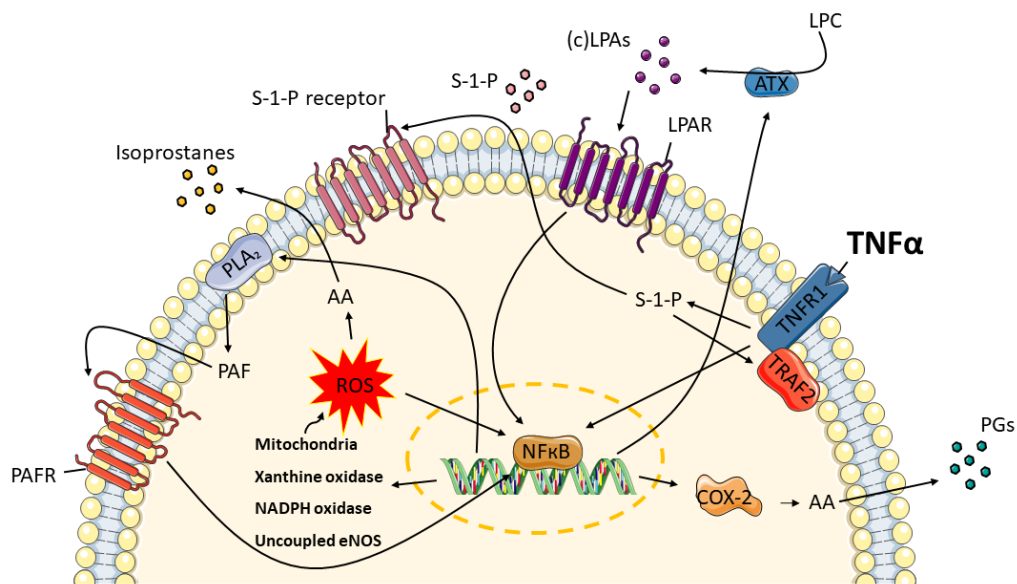


Figure 5 | TNF α induces the release of oxidative stress and inflammatory markers in endothelial cells. Exposure to TNF α , causes TNF signaling in the microvessels to produce ROS from endogenous sources: mitochondria, xanthine oxidase, NADPH oxidase and uncoupled eNOS. Sphingosine-1-phosphate (S-1-P) is needed in order for TNF receptor-associated factor 2 (TRAF2) to form a complex with the TNF receptor 1 (TNFR1). These lead to the conversion of arachidonic acid (AA) to isoprostanes and NF κ B activation. Moreover, AA is enzymatically converted by cyclooxygenase-2 (COX-2) to prostaglandins (PGs). At the same time, autotaxin (ATX) and phospholipase A₂ (PLA₂) are upregulated, resulting in the syntheses of lysophosphatidic acid (LPA) classes and platelet activating factor (PAF). Through their receptors, LPAs and PAF further promote the activation of COX-2.

Conclusions

We demonstrate bioactive lipid profiles can be readily detected from minor volumes of < 1 μ l of conditioned medium from microvessels-on-a-chip and display a more dynamic, less inflammatory response to TNF α compared to classical two-dimensional endothelial cell cultures. We can conclude that the response to TNF α resembles for the microvessels-on-a-chip more the human situation as described in the literature than the 2D endothelial cell culture. As the physiological readout of endothelial function is a critical aspect in using microvessels-on-a-chip for disease and drug research, the results suggest that the metabolic readout using metabolomics is more informative compared to morphological changes studied with imaging analyses of phenotypic changes. But it is the combination of both techniques,

Chapter V

metabolic readout using metabolomics and imaging analysis that may facilitate mechanistic studies and the detection and validation of biomarkers for microvascular disease at the systemic level. Furthermore, it will provide the information needed to understand microvascular destabilization and will generate a knowledge base for developing and testing personalized therapeutic interventions.

Data availability

All data generated or analysed during this study are included in this published article (and its Supplementary Information files).

Conflict of interest

TH is co-founder of MIMETAS and has some shares in MIMETAS. All other authors declare no conflict of interest related to the content of this manuscript.

Acknowledgements

This study was financially supported by the RECONNECT CVON Groot consortium, which is funded by the Dutch Heart Foundation. AJ and TH, AJvZ were supported by a ZonMW MKMD grant (114022501). AM and TH acknowledge the support by the NWO-TTW (IMMUNMET, grant number 16249). TH acknowledged the support by the TKI METABOCHIP project.

Author Contributions

Conceptualization: Abidemi Junaid, Anton Jan van Zonneveld and Thomas Hankemeier. Investigation: Abidemi Junaid, Johannes Schoeman, Wei Yang and Wendy Stam. Writing – original draft: Abidemi Junaid. Writing – review & editing: All authors. Supervision: Alireza Mashaghi, Anton Jan van Zonneveld and Thomas Hankemeier. Funding acquisition: Anton Jan van Zonneveld and Thomas Hankemeier.

References

1. Sedger, L.M. and M.F. McDermott, *TNF and TNF-receptors: From mediators of cell death and inflammation to therapeutic giants - past, present and future*. Cytokine Growth Factor Rev, 2014. **25**(4): p. 453-72.
2. Chimen, M., et al., *Monocyte Subsets Coregulate Inflammatory Responses by Integrated Signaling through TNF and IL-6 at the Endothelial Cell Interface*. Journal of Immunology, 2017. **198**(7): p. 2834-2843.
3. Torres-Castro, I., et al., *Human monocytes and macrophages undergo M1-type inflammatory polarization in response to high levels of glucose*. Immunology Letters, 2016. **176**: p. 81-89.
4. Green, L.A., et al., *Endogenous Transmembrane TNF-Alpha Protects Against Premature Senescence in Endothelial Colony Forming Cells*. Circ Res, 2016. **118**(10): p. 1512-24.
5. Masi, S., et al., *Mitochondrial oxidative stress, endothelial function and metabolic control in patients with type II diabetes and periodontitis: A randomised controlled clinical trial*. Int J Cardiol, 2018. **271**: p. 263-268.
6. Engin, A., *Endothelial Dysfunction in Obesity*. Adv Exp Med Biol, 2017. **960**: p. 345-379.
7. Rabelink, T.J., H.C. de Boer, and A.J. van Zonneveld, *Endothelial activation and circulating markers of endothelial activation in kidney disease*. Nat Rev Nephrol, 2010. **6**(7): p. 404-14.
8. van Zonneveld, A.J., et al., *Inflammation, vascular injury and repair in rheumatoid arthritis*. Ann Rheum Dis, 2010. **69 Suppl 1**: p. i57-60.
9. Pisoschi, A.M. and A. Pop, *The role of antioxidants in the chemistry of oxidative stress: A review*. Eur J Med Chem, 2015. **97**: p. 55-74.
10. Cai, H. and D.G. Harrison, *Endothelial dysfunction in cardiovascular diseases: the role of oxidant stress*. Circ Res, 2000. **87**(10): p. 840-4.
11. Blaser, H., et al., *TNF and ROS Crosstalk in Inflammation*. Trends Cell Biol, 2016. **26**(4): p. 249-261.
12. Poussin, C., et al., *3D human microvessel-on-a-chip model for studying monocyte-to-endothelium adhesion under flow - application in systems toxicology*. ALTEX, 2019.
13. Morrow, J.D., et al., *A series of prostaglandin F2-like compounds are produced in vivo in humans by a non-cyclooxygenase, free radical-catalyzed mechanism*. Proc Natl Acad Sci U S A, 1990. **87**(23): p. 9383-7.
14. Ridker, P.M., et al., *Established and emerging plasma biomarkers in the prediction of first atherothrombotic events*. Circulation, 2004. **109**(25 Suppl 1): p. IV6-19.

Chapter V

15. Moutzouri, E., et al., *Comparison of the effect of simvastatin versus simvastatin/ezetimibe versus rosuvastatin on markers of inflammation and oxidative stress in subjects with hypercholesterolemia*. *Atherosclerosis*, 2013. **231**(1): p. 8-14.
16. Vassalle, C., et al., *Oxidative stress and its association with coronary artery disease and different atherogenic risk factors*. *J Intern Med*, 2004. **256**(4): p. 308-15.
17. Esposito, E. and S. Cuzzocrea, *TNF-Alpha as a Therapeutic Target in Inflammatory Diseases, Ischemia-Reperfusion Injury and Trauma*. *Current Medicinal Chemistry*, 2009. **16**(24): p. 3152-3167.
18. Ackerman, S.J., et al., *Polyunsaturated lysophosphatidic acid as a potential asthma biomarker*. *Biomark Med*, 2016. **10**(2): p. 123-35.
19. Jaffe, E.A., et al., *Culture of human endothelial cells derived from umbilical veins. Identification by morphologic and immunologic criteria*. *J Clin Invest*, 1973. **52**(11): p. 2745-56.
20. Stroka, K.M. and H. Aranda-Espinoza, *Endothelial cell substrate stiffness influences neutrophil transmigration via myosin light chain kinase-dependent cell contraction*. *Blood*, 2011. **118**(6): p. 1632-1640.
21. Huveneers, S., M.J.A.P. Daemen, and P.L. Hordijk, *Between Rho(k) and a Hard Place The Relation Between Vessel Wall Stiffness, Endothelial Contractility, and Cardiovascular Disease*. *Circulation Research*, 2015. **116**(5): p. 895-908.
22. Huveneers, S., M.J. Daemen, and P.L. Hordijk, *Between Rho(k) and a hard place: the relation between vessel wall stiffness, endothelial contractility, and cardiovascular disease*. *Circ Res*, 2015. **116**(5): p. 895-908.
23. Baeyens, N., et al., *Endothelial fluid shear stress sensing in vascular health and disease*. *J Clin Invest*, 2016. **126**(3): p. 821-8.
24. Wevers, N.R., et al., *A perfused human blood-brain barrier on-a-chip for high-throughput assessment of barrier function and antibody transport*. *Fluids Barriers CNS*, 2018. **15**(1): p. 23.
25. van Duinen, V., et al., *96 perfusable blood vessels to study vascular permeability in vitro*. *Sci Rep*, 2017. **7**(1): p. 18071.
26. van Duinen, V., et al., *96 perfusable blood vessels to study vascular permeability in vitro*. *Scientific Reports*, 2017. **7**.
27. Koutsiaris, A.G., et al., *Volume flow and wall shear stress quantification in the human conjunctival capillaries and post-capillary venules in vivo*. *Biorheology*, 2007. **44**(5-6): p. 375-386.

28. Schoeman, J.C., et al., *Development and application of a UHPLC-MS/MS metabolomics based comprehensive systemic and tissue-specific screening method for inflammatory, oxidative and nitrosative stress*. Anal Bioanal Chem, 2018. **410**(10): p. 2551-2568.
29. Chang, M.S., et al., *Phorbol 12-myristate 13-acetate upregulates cyclooxygenase-2 expression in human pulmonary epithelial cells via Ras, Raf-1, ERK, and NF-kappa B, but not p38 MAPK, pathways*. Cellular Signalling, 2005. **17**(3): p. 299-310.
30. Wong, M.S.K. and P.M. Vanhoutte, *COX-mediated endothelium-dependent contractions: from the past to recent discoveries*. Acta Pharmacologica Sinica, 2010. **31**(9): p. 1095-1102.
31. Dworski, R., et al., *Assessment of oxidant stress in allergic asthma by measurement of the major urinary metabolite of F2-isoprostane, 15-F2t-IsoP (8-iso-PGF2alpha)*. Clin Exp Allergy, 2001. **31**(3): p. 387-90.
32. Trebaticka, J., et al., *Cardiovascular Diseases, Depression Disorders and Potential Effects of Omega-3 Fatty Acids*. Physiological Research, 2017. **66**(3): p. 363-382.
33. Gezginci-Oktayoglu, S., N. Orhan, and S. Bolkent, *Prostaglandin-E-1 has a protective effect on renal ischemia/reperfusion-induced oxidative stress and inflammation mediated gastric damage in rats*. International Immunopharmacology, 2016. **36**: p. 142-150.
34. Ohmura, T., et al., *Regulation of lung endothelial permeability and inflammatory responses by prostaglandin A2: role of EP4 receptor*. Molecular Biology of the Cell, 2017. **28**(12): p. 1622-1635.
35. Rokach, J., et al., *The isoprostanes: A perspective*. Prostaglandins & Other Lipid Mediators, 1997. **54**(6): p. 823-851.
36. Durackova, Z., *Some Current Insights into Oxidative Stress*. Physiological Research, 2010. **59**(4): p. 459-469.
37. Nakano, J. and J.M. Kessinger, *Effects of 8-isoprostaglandin E1 on the systemic and pulmonary circulations in dogs*. Proc Soc Exp Biol Med, 1970. **133**(4): p. 1314-7.
38. Karshovska, E., et al., *Endothelial specific autotaxin in atherosclerosis*. European Heart Journal, 2018. **39**: p. 1404-1405.
39. Khandoga, A.L., et al., *Lysophosphatidic acid-induced platelet shape change revealed through LPA(1-5) receptor-selective probes and albumin*. Platelets, 2008. **19**(6): p. 415-27.
40. Biermann, D., et al., *Impact of AT2 receptor deficiency on postnatal cardiovascular development*. PLoS One, 2012. **7**(10): p. e47916.
41. Yang, B., et al., *The effect of lysophosphatidic acid on Toll-like receptor 4 expression and the nuclear factor-kappa B signaling pathway in THP-1 cells*. Molecular and Cellular Biochemistry, 2016. **422**(1-2): p. 41-49.

Chapter V

42. Ninou, J., C. Magkrioti, and V. Aidinis, *Autotaxin in Pathophysiology and Pulmonary Fibrosis*. *Frontiers in Medicine*, 2018. **5**.
43. Palmetshofer, A., S.C. Robson, and V. Nehls, *Lysophosphatidic acid activates nuclear factor kappa B and induces proinflammatory gene expression in endothelial cells*. *Thrombosis and Haemostasis*, 1999. **82**(5): p. 1532-1537.
44. Tsukahara, T., H. Haniu, and Y. Matsuda, *Cyclic Phosphatidic Acid Inhibits Alkyl-Glycerophosphate-Induced Downregulation of Histone Deacetylase 2 Expression and Suppresses the Inflammatory Response in Human Coronary Artery Endothelial Cells*. *International Journal of Medical Sciences*, 2014. **11**(9): p. 955-961.
45. Alvarez, S.E., et al., *Sphingosine-1-phosphate is a missing cofactor for the E3 ubiquitin ligase TRAF2*. *Nature*, 2010. **465**(7301): p. 1084-U149.
46. Ramakrishnan, A.V.K.P., et al., *Platelet activating factor: A potential biomarker in acute coronary syndrome?* *Cardiovascular Therapeutics*, 2017. **35**(1): p. 64-70.
47. Lee, J., et al., *In vitro Toxicity Testing of Nanoparticles in 3D Cell Culture*. *Small*, 2009. **5**(10): p. 1213-1221.
48. Bhagyalakshmi, A., et al., *Fluid Shear-Stress Stimulates Membrane Phospholipid-Metabolism in Cultured Human Endothelial-Cells*. *Journal of Vascular Research*, 1992. **29**(6): p. 443-449.
49. Liu, B., et al., *RhoA and Membrane Fluidity Mediates the Spatially Polarized Src/FAK Activation in Response to Shear Stress*. *Scientific Reports*, 2014. **4**.
50. Schulz, E., T. Gori, and T. Munzel, *Oxidative stress and endothelial dysfunction in hypertension*. *Hypertens Res*, 2011. **34**(6): p. 665-73.
51. Shiraki, A., et al., *The glucagon-like peptide 1 analog liraglutide reduces TNF-alpha-induced oxidative stress and inflammation in endothelial cells*. *Atherosclerosis*, 2012. **221**(2): p. 375-82.
52. Ryu, Y., M.J. Reid, and K.V. Thomas, *Liquid chromatography-high resolution mass spectrometry with immunoaffinity clean-up for the determination of the oxidative stress biomarker 8-iso-prostaglandin F2alpha in wastewater*. *J Chromatogr A*, 2015. **1409**: p. 146-51.
53. Vulto, P., et al., *Phaseguides: a paradigm shift in microfluidic priming and emptying*. *Lab on a Chip*, 2011. **11**(9): p. 1596-1602.
54. Wishart, D.S., et al., *HMDB 4.0: the human metabolome database for 2018*. *Nucleic Acids Research*, 2018. **46**(D1): p. D608-D617.
55. Wishart, D.S., et al., *HMDB 3.0-The Human Metabolome Database in 2013*. *Nucleic Acids Research*, 2013. **41**(D1): p. D801-D807.

Chapter V

56. Wishart, D.S., et al., *HMDB: the human metabolome database*. Nucleic Acids Research, 2007. **35**: p. D521-D526.

57. Wishart, D.S., et al., *HMDB: a knowledgebase for the human metabolome*. Nucleic Acids Research, 2009. **37**: p. D603-D610.

Supplementary Tables

Supplementary Table 1 | An overview of the concentrations of the calibration solution.

Bioactive lipid	Stock concentration (nM)								
	C9	C8	C7	C6	C5	C4	C3	C2	C1
PGF1 α	53.3	26.7	13.3	6.7	3.3	1.7	0.8	0.4	0.2
PGF2 α	53.3	26.7	13.3	6.7	3.3	1.7	0.8	0.4	0.2
PGF3 α	53.3	26.7	13.3	6.7	3.3	1.7	0.8	0.4	0.2
PGE2	53.3	26.7	13.3	6.7	3.3	1.7	0.8	0.4	0.2
PGE1	53.3	26.7	13.3	6.7	3.3	1.7	0.8	0.4	0.2
PGD2	53.3	26.7	13.3	6.7	3.3	1.7	0.8	0.4	0.2
13, 14-dihydro-PGF2 α	41.9	21.0	10.5	5.2	2.6	1.3	0.7	0.3	0.2
PGA2	53.3	26.7	13.3	6.7	3.3	1.7	0.8	0.4	0.2
8-iso-13, 14-dihydro-PGF2 α	53.3	26.7	13.3	6.7	3.3	1.7	0.8	0.4	0.2
8-iso-PGF2 α	53.3	26.7	13.3	6.7	3.3	1.7	0.8	0.4	0.2
8-iso-PGE2	53.3	26.7	13.3	6.7	3.3	1.7	0.8	0.4	0.2
8-iso-PGE1	53.3	26.7	13.3	6.7	3.3	1.7	0.8	0.4	0.2
5-iPF2 α	53.3	26.7	13.3	6.7	3.3	1.7	0.8	0.4	0.2
8, 12-iPF2 α IV	53.3	26.7	13.3	6.7	3.3	1.7	0.8	0.4	0.2
LPA C20:4	2400.0	1200.0	600.0	300.0	150.0	75.0	37.5	18.8	9.4
LPA C16:0	2400.0	1200.0	600.0	300.0	150.0	75.0	37.5	18.8	9.4
LPA C18:1	3200.0	1600.0	800.0	400.0	200.0	100.0	50.0	25.0	12.5
LPA C18:0	2666.7	1333.3	666.7	333.3	166.7	83.3	41.7	20.8	10.4
cLPA C18:1	2400.0	1200.0	600.0	300.0	150.0	75.0	37.5	18.8	9.4
S-1-P C18:1	8000.0	4000.0	2000.0	1000.0	500.0	250.0	125.0	62.5	31.3
Spha C18:1	9600.0	4800.0	2400.0	1200.0	600.0	300.0	150.0	75.0	37.5
Spha C18:0	9600.0	4800.0	2400.0	1200.0	600.0	300.0	150.0	75.0	37.5
PAF C16:0	1333.3	666.7	333.3	166.7	83.3	41.7	20.8	10.4	5.2

Chapter V

Supplementary Table 2 | References regarding the action of bioactive lipids on inflammation, platelets, vascular tone and angiogenesis.

Bioactive lipid	PMID
PGF1 α	3110148
PGF2 α	11438482 6999547 1415588
PGF3 α	16297610
PGE2*	30112590
PGE1	6999547 24431002 12494264
PGD2	6999547 30734298 29671869
13, 14-dihydro-PGF2 α	
PGA2	6999547 15723383
8-iso-13, 14-dihydro-PGF2 α	
8-iso-PGF2 α *	11344105 15640282 18802021 10711349
8-iso-PGE2	12716476 10711349 24646155
8-iso-PGE1	10711349
5-iPF2 α	
8, 12-iPF2 α IV	
LPA C14:0	25825155 30928673
LPA C16:1	25825155 30928673
LPA C22:6*	25825155 30928673
LPA C18:2	25825155 30928673
LPA C20:4	25825155 30928673
LPA C22:5*	25825155 30928673
LPA C16:0	25825155 30928673
LPA C18:1	25825155 30928673
LPA C22:4	25825155 30928673
cLPA C20:4	25013374 18554524
LPA C18:0	25825155 30928673
cLPA C18:2	25013374 18554524
cLPA C16:0	25013374 18554524
cLPA C18:1	25013374 18554524
cLPA C18:0	25013374 18554524
S-1-P C18:1	28609704 31049553 20577214 27565080
Sph C18:1	28609704 31049553 20577214 27565080
Spha C18:0	
PAF C16:0	17588613 12038971

*Validated markers of oxidative stress.



Chapter V

V